



Comparison of degradation mechanism of electrochemical oxidation of di- and tri-nitrophenols on Bi-doped lead dioxide electrode: Effect of the molecular structure

Yuan Liu, Huiling Liu*, Jun Ma, Xi Wang

State Key Laboratory of Urban Water Resources and Environment (SKLUWRE), Department of Environmental Science & Engineering, Harbin Institute of Technology, Huanghe Road 73, Nangang District, Harbin 150090, China

ARTICLE INFO

Article history:

Received 1 March 2009

Received in revised form 10 May 2009

Accepted 27 May 2009

Available online 6 June 2009

Keywords:

Nitrophenol

Electrochemical oxidation

Mechanism

Bi-doped lead dioxide electrode

Molecular structure

ABSTRACT

In the present work, the effect of molecular structures of di- and tri-nitrophenols on electrochemical degradation has been investigated on Bi-doped lead dioxide electrodes in terms of cyclic voltammetry and bulk electrolysis. The results of SEM and AFM displayed a porous structure with small-sized crystal particles and compact crystalline structure of Ti/Bi-PbO₂. These nitrophenols were believed to be mainly degraded by means of indirect oxidation due to the low anodic oxidation currents observed in cyclic voltammetries and large amount of oxidants. And the absence of polymeric adhesive compounds formed and deposited on the surface of electrodes indicated the high electrocatalytic activity of Ti/Bi-PbO₂ for decomposing organics. Within the present experimental conditions used, almost complete elimination of nitrophenols was achieved. The electrochemical oxidation of them followed in the order: 2,6-dinitrophenol > 2,5-dinitrophenol > 2,4-dinitrophenol > 2,4,6-trinitrophenol. The relationship between electrochemical oxidation rate and the molecular structure of nitrophenols was discussed. The results of LC/MS and HPLC suggested that three kinds of intermediates were generated, i.e., polyhydroxylated intermediates, reduction products of nitrophenols and carboxylic acids. The possible degradation pathways of nitrophenols were proposed. The denitration and substitution by hydroxyl radicals on aromatic rings seemed to be the first stage. As a consequence, the formation of polyhydroxylated intermediates took place. These compounds were successively oxidized into catechol, resorcinol and hydroquinone, as well as reduced to aminophenols, followed by the opening of aromatic rings and the formation of a series of carboxylic acids. Finally, these carboxylic acids were oxidized into CO₂ and H₂O.

© 2009 Elsevier B.V. All rights reserved.

1. Introduction

Nitrophenols (NPs) which have been detected in urban and agricultural wastes are anthropogenic, toxic, inhibitory and bio-refractory organic compounds [1] and are considered as hazardous substances and priority toxic pollutants by the United States Environmental Protection Agency (USEPA) [2]. 2,4-Dinitrophenol (2,4-DNP), 2,5-dinitrophenol (2,5-DNP), 2,6-trinitrophenol (2,6-DNP) and 2,4,6-TNP (2,4,6-TNP) are among the most common and versatile industrial organic compounds with extensive application as pesticides, pigments, dyes, pharmaceuticals and explosive materials [3–9]. With respect to their biorecalcitrant properties, biological methods seem ineffective or require long incubation time on the degradation of these compounds [10–13]. Hence, it is

of significant importance to develop new treatment technologies for the decomposition and mineralization of these organic contaminants in wastewater. Up until date, alternative approaches especially advanced oxidation processes (AOPs) have been intensively investigated [8,14–17]. However, few studies focus on electrocatalytic oxidation (ECO) which is one of the most effective AOPs [18–20].

Electrocatalytic oxidation appears as one of the most promising technologies for the treatment of wastewater containing small amounts of aromatic compounds. The main advantages of the ECO processes include environmental compatibility, versatility, energy efficiency, safety, selectivity, amenability to automation and cost effectiveness [21]. The use of high performance anodic materials like lead dioxide (PbO₂) electrode can achieve high efficiency and lower the operating cost. PbO₂ has been extensively used to decompose organic contaminants owing to its high electrical conductivity, high oxygen overpotential and chemical inertness and low cost [22–26]. A general scheme for the ECO degradation of

* Corresponding author. Tel.: +86 451 53625118.

E-mail address: hliu2002@163.com (H. Liu).

organic compounds on metal oxide electrodes (MO_x) has been proposed [27], including the discharge of water molecules on the surface of electrodes to generate hydroxyl radicals and successive reactions between hydroxyl radicals and organic compounds in solutions.

The electrocatalytic properties of electrodeposited PbO_2 are strongly affected by doping species present in the deposition bath, especially metal cations, which can change certain characteristics of the PbO_2 electrode, including catalytic activity and O-atom transfer properties [28–30]. In our previous studies, we investigated Bi-doped PbO_2 electrode which displayed superior electrocatalytic activities than traditional PbO_2 electrode [31,32].

So far, many researchers have been carrying out a large number of investigations on the ECO of *p*-NP, but few researches focus on the multi-substituted nitrophenols [33–35]. Up to now, the systematic investigations about the ECO mechanisms of 2,4-DNP, 2,5-DNP and 2,6-DNP as well as 2,4,6-TNP have not yet been reported. Therefore, the mechanisms involved in the electrocatalytic oxidation processes of these NPs are not fully understood.

The goal of the present work was attempted to use electrocatalytic oxidation on Bi-doped PbO_2 electrode for the treatment of 2,4-DNP, 2,5-DNP, 2,6-DNP and 2,4,6-TNP aqueous solutions. The electrocatalytic oxidation of NPs was investigated in terms of cyclic voltammetry and bulk electrolysis. Oxidants, such as hydroxyl radical, hydrogen peroxide and hypochlorite ion, were monitored. The kinetics of electrocatalytic oxidation of NPs were investigated, as well as the formation of intermediates, by means of liquid chromatograph and mass spectrometry. The mechanism of degradation was investigated in detail in view of the molecular structure and a distinct degradation pathway was proposed.

2. Experimental

2.1. Materials

2,4-DNP, 2,5-DNP, 2,6-TNP and 2,4,6-TNP were purchased from Aldrich (AR grade) and used as received. All other chemicals were analytical grade and used without further purification. Solutions were prepared using deionized Milli-Q water. The preparation of Bi-doped lead dioxide electrodes (Ti/Bi- PbO_2) was given in detail in our previous work [32].

2.2. Analysis

The morphology of the Bi- PbO_2 electrode was examined using a scanning electronic microscopy (SEM; USA Camscan MX2600FE). This instrument incorporated an energy dispersive X-ray analysis (EDX) for elemental analysis. An atomic force microscopy (AFM) imaging was performed under ambient condition using a Digital Instruments (Veeco) Dimension-3100 unit with Nanoscope IIIa controller, operated in contact mode. Standard silicon nitride probes (Veeco part number NP), having a force constant of approximately 0.58 N m^{-1} , were used.

Cyclic voltammetry were tested with a standard three-electrode cell using a computer control potentiostat/galvanostat model 263A (Princeton Applied Research). Bi-doped lead dioxide electrode was used as working electrode, a platinum sheet as counter electrode and a saturated calomel electrode as a reference electrode placed in Luggin capillary which was near the working electrode. The exposed apparent area of the working electrode was 1 cm^2 . The cyclic voltammetry were performed at room temperature. The electrolytes used in the voltammetry measurements are the same as those in bulk electrolysis.

The concentrations of NPs were measured with a LC-10A High Performance Liquid Chromatograph (HPLC) equipped with a UV-spectrophotometer (190–360 nm). Aliquots of $10 \mu\text{L}$ were injected

automatically into the HPLC to determine the concentration of NPs, using a mobile phase of mixture of 50% acetonitrile and 0.5% phosphoric acid. The separation was performed using a Vp-ODS reversed phase column at the flow rate of 1 mL min^{-1} under 10.7 MPa pressure and column temperature of 303 K. Before the analysis, the mobile phase was filtered and sonicated in order to remove dissolved gas. The detection wavelength was 260 nm.

Aromatic compounds were also monitored by the same HPLC. The mobile phase was the mixture of 70% methanol/30% water/0.5% phosphoric acid. The separation was performed using a Vp-ODS reversed phase column at the flow rate of 0.5 mL min^{-1} . In this case, UV wavelength was set to 280 nm.

Electrolysis intermediates, especially polyhydroxylated intermediates, were identified by liquid chromatography/mass spectrometry (LC/MS, Finigan LCQ DEXP MAX) equipped with an ESI source. As for the LC condition, methanol/water = 1:1 was used as mobile phase and flow rate was set to 0.2 mL min^{-1} without a separation column. Full scale MS spectra both in positive and negative modes in the mass range between 50 and 500 *m/z* were recorded. The following operation parameters were used: capillary voltage +4.0 keV, capillary temperature 548 K, drying gas heater temperature 623 K, dwell time 5 ms.

Carboxylic acids were determined by this HPLC equipped a HPICE-ASI DIONEX ICNPAC column (mobile phase, 0.15% phosphoric acid; flow rate, 0.8 mL min^{-1}). UV wavelength was set to 210 nm.

The determination of the concentration of nitrogen inorganic ions (NO_3^- , NO_2^-) were measured with an ion chromatograph (DIONEX ICS-3000) equipped with an electrical conductivity detector (ECD). Aliquots of $10 \mu\text{L}$ were injected into the IC, and carried with a mobile phase containing 1.7 mM NaHCO_3 and 1.8 mM Na_2CO_3 . The separation was performed using an AS11-HC phase column at the flow rate of 1.2 mL min^{-1} under 1885 psi. Ammonium was analyzed according to Kjeldahl method. COD was measured by a titrimetric method using dichromate as the oxidant in acidic solution at 458 K for 2 h (Hachi).

The fluorescence intensity was measured on JASCO FP-6500 spectrofluorimeter to determine the amount of $\cdot\text{OH}$. The fluorescence intensity is measured at 431 nm with excitation at 313 nm and the relative fluorescence intensity was proportional to the amount of $\cdot\text{OH}$. The detail measurement was described in the literature [36]. The concentration of hydrogen peroxide accumulated during electrolysis was determined by measuring the light absorption of titanous-hydrogen peroxide colored complex at $\lambda = 420 \text{ nm}$ [37]. The concentration of total oxidants in the same solutions was determined by iodometric titration [38]. The concentration of hypochlorite ion was obtained as difference between the concentration of total oxidants and hydrogen peroxide.

2.3. Electrocatalytic oxidation

The electrocatalytic oxidation experiments were carried out by batch processes and the apparatus was mainly consisted of a DC power supply, a water bath equipped a magnetic stirrer and a single-compartment glass reactor. The anode (Ti/Bi- PbO_2) and cathode (stainless steel sheet) were positioned vertically and parallel to each other with a distance of 1 cm.

The initial concentrations of NPs were selected as 0.36 mM with a volume of 200 mL. The initial pH of the solutions was adjusted to 4.0 ± 0.1 using 0.05 M H_2SO_4 and the reaction temperature was kept at 313 K. The current density was set at 20 mA cm^{-2} during all the experimental runs. The concentrations of electrolytes were kept at 0.05 M Na_2SO_4 and 0.01 M NaCl. During the experiments, samples were drawn from the reactor at certain intervals and then analyzed. All of experimental runs were performed in triplicate and each data was a mean of these three determinations.

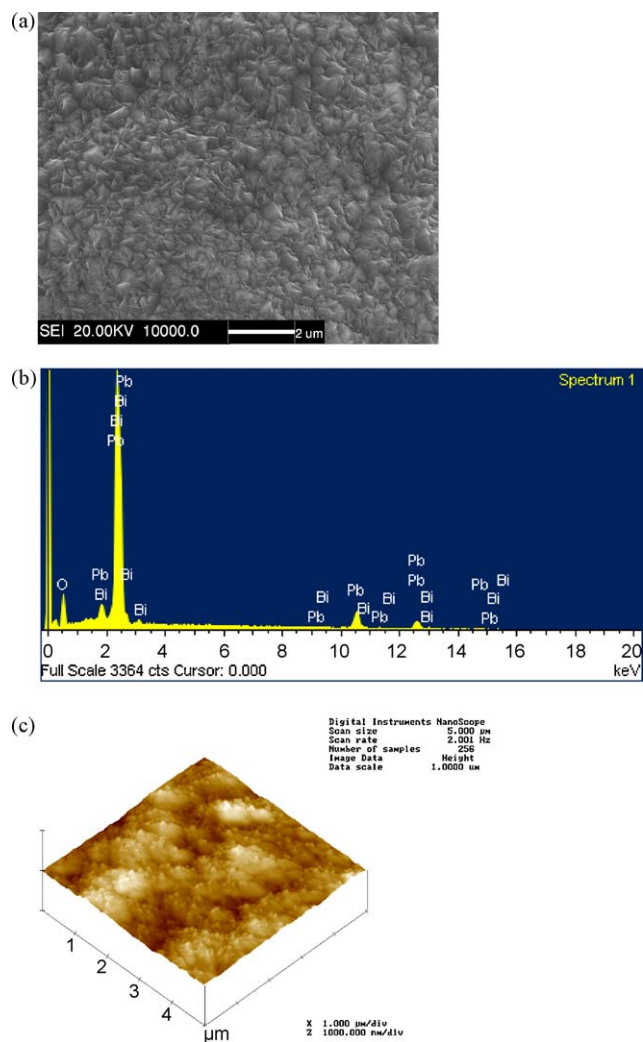


Fig. 1. SEM micrograph (a), EDX elemental analysis (b) and AFM image of Bi-PbO₂ electrode (c).

3. Results and discussion

3.1. Characteristics of Ti/Bi-PbO₂ anode

The SEM micrograph of Ti/Bi-PbO₂ anode is shown in Fig. 1, as well as the EDX elemental analysis of this anode. Ti/Bi-PbO₂ anode has a porous structure with small-sized crystal particles and a very compact crystalline structure (Fig. 1a). The crystal size of this anode was ca. 17.491 nm in terms of our previous studies [32]. The results of EDX confirmed that Bi atoms were doped into the PbO₂ films. Fig. 1c shows the AFM image of Ti/Bi-PbO₂ anode, which displays a uniform island-like structure. It believes that the larger roughness and smaller crystalline of Ti/Bi-PbO₂ anode was beneficial for adsorbing water or organic molecules. Large roughness and small crystalline of this anode favored increasing its specific surface area. As we know, large specific surface area is one of the characteristics of benign catalysis. PbO₂ strong adsorption property so that water is more readily adsorbed on the surface of electrode with large specific surface area. The more the water molecules are adsorbed, the more hydroxyl radicals are electro-generated by means of water discharge. Consequently, organic compounds are easier to be decomposed. Therefore, Ti/Bi-PbO₂ anode is believed to be suitable for the elimination of organic contaminants.

As reported in previous studies [39,40], oxidants in electro-catalytic systems played an important role in the process of organic

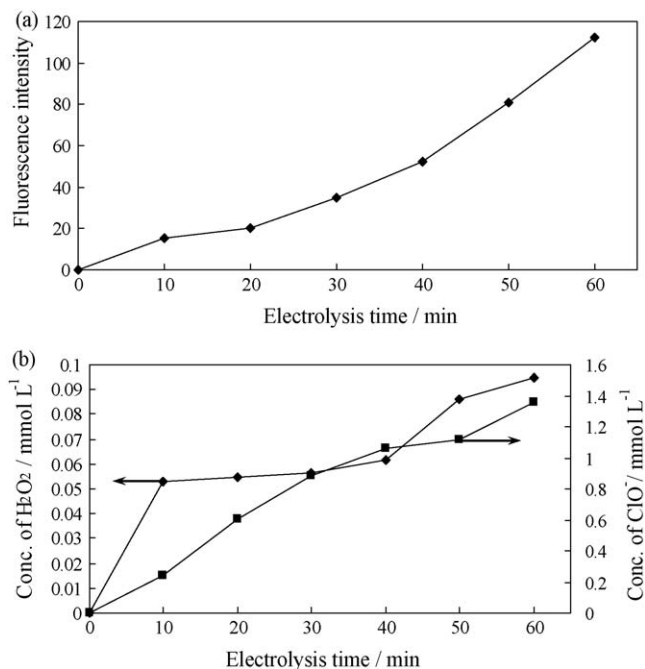
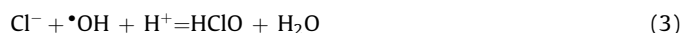
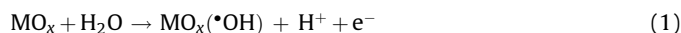


Fig. 2. Variation of concentration of oxidants in the electrochemical system (a) fluorescence intensity, (b) H₂O₂ and ClO⁻, pH 4; current density = 20 mA cm⁻²; temperature = 313 K; 0.05 M Na₂SO₄ and 0.01 M NaCl.

pollutants degradation. The indirect oxidation through electro-generated oxidants is mainly attributed to hydrogen peroxide and peroxodisulfate ion when working with Na₂SO₄ as electrolyte and to hypochlorite ion when using NaCl. In our previous study, we testified the existence of these oxidants in acidic condition [32].

In this work, the oxidants including hydroxyl radical, hydrogen peroxide and hypochlorite ion were also determined qualitatively and quantitatively. The evolutions of the concentration of oxidants are presented in Fig. 2. The variation of fluorescence intensity as a function of electrolysis time shown in Fig. 2a indicated that [•]OH generated in the present experimental system. H₂O is assumed to be discharged on the surface of this electrode to form adsorbed hydroxyl radicals as shown in Eq. (1). In addition, the formation of hydrogen peroxide and hypochlorite ion could be expressed as following Eqs. ((2)–(3)):



The recombination of hydroxyl radicals would result in the formation of H₂O₂, and the interaction between Cl⁻ and hydroxyl radicals would generate ClO⁻. In addition, Cl₂ was also generated due to the discharge of Cl⁻ at anode. Therefore, the formation of hypochlorite ion was also ascribed to the hydrolyzation of Cl₂ [41], which has been widely recognized as the possible mechanism in the presence of Cl⁻ during electrolysis. The reactions and processes involved in the generation of oxidants and contaminants oxidation could be summarized and displayed in Fig. 3. In this figure, one can see the whole pathways on the generation of hydroxyl radicals, hydrogen peroxide and hypochlorite ion, as well as the oxidation of organic compounds by these oxidants.

Especially, though Eq. (1) displayed the generation of hydroxyl radicals on the surface of Bi-doped lead dioxide electrode, the mechanism of the generation of hydroxyl radicals could be more complex than this assumption. Pavlov et al. [42,43] have done large

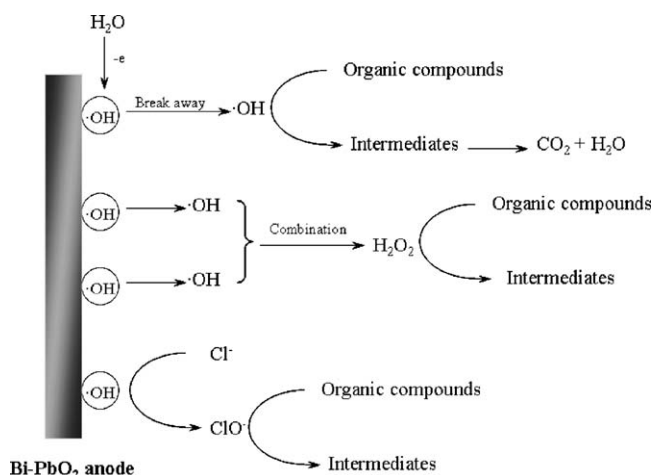


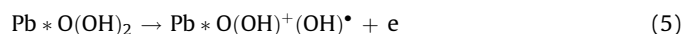
Fig. 3. Scheme of the reactions and processes involved in the generation of oxidants and contaminants oxidation on Bi-doped lead dioxide anode.

amount of works to study the relationship between the structure of PbO₂ electrode and the generation of ·OH. He and co-workers proposed a mechanism which interpreted the electrochemical processes taking place on the lead dioxide electrode. They suggested a gel–crystal system shown as following equilibrium process:



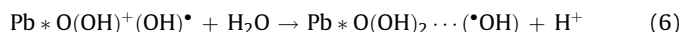
In this system, crystal zones were built of PbO₂ and gel zones were composed of hydrated lead dioxide, denoted as PbO(OH)₂. The α- and β-PbO₂ crystals have a layered structure built of “PbO₆” octahedrons interconnected into chains which are zigzag for the former and linear for the latter. Upon hydration, β-PbO₂ linear chains are preserved to a certain extent, turning into the polymer hydrated chains presented in pervious work [44]. The polymer chains have electron and proton conductivity [42]. As the distance between the Pb⁴⁺ ions in the polymer chain is relatively small, electrons easily jump from one Pb⁴⁺ ion to another, overcoming small energy barriers. So do the H⁺ ions passing from one OH⁻ group to the adjacent one along the polymer chain. Electrons and protons may jump from one polymer chain to another if the distance between them is short. On the other hand, part of the polymer chain is connected to crystal zones. Therefore, electrons move linearly along the chains in the gel zones, while their movement is free throughout the volume of the crystal zones [43]. In addition, the hydrated layer interacts with the solution, exchanging cations, anions, and water molecules with it [42]. This makes the hydrated layer an open system.

In light of the gel–crystal concept for the structure of PbO₂ surface, Pavlov and Manahov [43] proposed that the oxygen electrochemical reaction proceeded on a certain number of active centers, which are denoted with Pb*O(OH)₂. Upon anodic polarization, when the potential of the lead dioxide electrode exceeds a certain value, an electrochemical reaction proceeds in the active centers:



The OH⁻ groups have different positions in the polymer chains with regard to the Pb⁴⁺ and Pb²⁺ ions. It can be assumed that, in certain structure configurations, electrons of the OH⁻ groups may jump into polymer chains and pass through the anodic layer. The movement of electrons along the polymer chains and the crystal zones result in the formation of electric current passing through the electrode. The active centers are charged positively. Their electric charge is neutralized through the chemical reaction as

following:



Where “...” represents the weak bond between the hydroxyl radicals and the active centers. Hence, the active centers contain hydroxyl radicals. This phenomenon is in its essence adsorption of hydroxyl radicals by the active centers. It could be expected that some of the adsorbed hydroxyl radicals would break away from the active centers and leave them. As a consequence, hydroxyl radicals are formed and would react with contaminants in solutions. Moreover, the existence of hydrogen peroxide could be interpreted in terms of the recombination of hydroxyl radicals. If the potential increased further, oxygen formed and evolved from the surface of anode, which was considered as side reaction of hydroxyl radical's generation. Though this species is characterized as high oxidative capacity, it is impossible to oxidize organic compounds in our electrolysis systems due to its easy evolution.

On the other hand, the incorporation of Bi into the surface of lead dioxide films is in favor of improving the formation of hydroxyl radicals [32]. Popović et al. [30,45] pointed out that Bi(V) sites were active centers which could absorb water molecules and promote anodic O-transfer reactions. In our previous studies [32], we investigated the different doping of metal element on the activities of lead dioxide electrodes. Incorporation of Bi into the surface of lead dioxide film would diminish the size of crystal of lead dioxide and increase the specific surface area of lead dioxide electrode. In addition, the incorporation of Bi would enhance the oxygen evolution overpotential of lead dioxide. These characteristics make the Bi-doped lead dioxide electrode more suitable to produce hydroxyl radicals and oxidize organic compounds.

3.2. Voltammetric study

Fig. 4 shows the cyclic voltammograms (CVs, second cycle) of 2,4-DNP, 2,5-DNP, 2,6-DNP and 2,4,6-TNP in the absence and presence of NPs. As it can be observed, there was a new anodic current peak appeared during the positive sweep for each NP and a pronounced increase in the current density between two kinds of solutions with and without NPs. In addition, another anodic current peak was observed at ca. +0.83 V (vs SCE) comparing with the first sweep (data not shown). It could be ascribed to the formation of HClO due to the hydrolyzation of Cl₂ which was generated in the first sweep. The new anodic current peaks were observed for 2,4-DNP, 2,5-DNP, 2,6-DNP and 2,4,6-TNP at +1.5 V (vs SCE), +1.6 V (vs SCE), +1.63 V (vs SCE) and +1.4 V (vs SCE), respectively, which might correspond to the direct oxidation of these compounds on the surface of anode. However, these peaks were small which suggested that the direct oxidation did not play an important role. Moreover, as the number of cycles increased, the shape of all CVs kept constant (data not shown), especially the peak potential and peak current, which indicated that there were no polymeric adhesive compounds formed and deposited on the surface of electrode in the present work. Cañizares et al. [33] reported that the peaks decreased in size with the number of cycles in the course of cyclic voltammetry of 2,4-DNP on BDD anode. The decrease in size might be attributed to electrode fouling which was resulted from the formation of polymers on the surface of anode. This differentiation indicates that the electrocatalytic behavior of Bi-doped PbO₂ is distinct from that of BDD. In addition, the current densities in the presence of NPs were larger than those in blank solutions. The phenomena could be explained as follows. As we know, lead dioxide electrode belongs to ‘nonactive’ electrodes [46] so that H₂O is assumed to be discharged on the surface of this electrode to form adsorbed hydroxyl radicals as mentioned above [27,47]. The absorbed hydroxyl radicals would react with organic

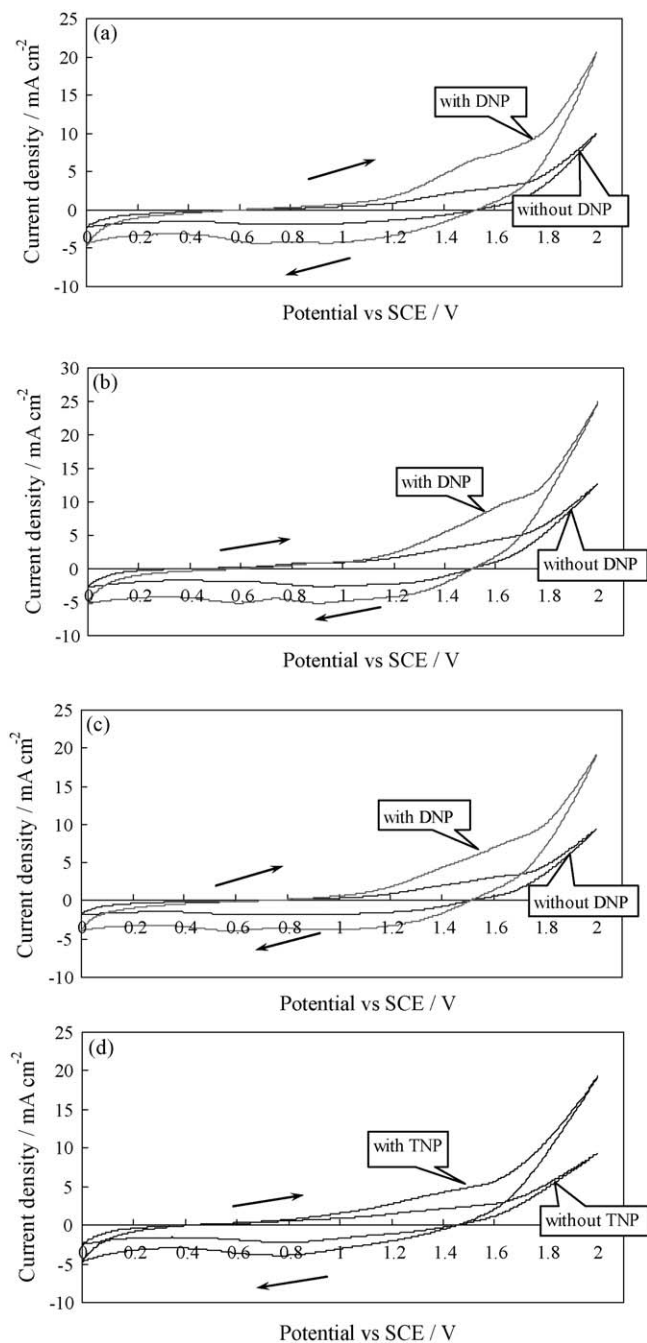


Fig. 4. Cyclic voltammograms (second cycle) on Bi-doped PbO₂ electrode of (a) 2,4-DNP, (b) 2,5-DNP, (c) 2,6-DNP and (d) 2,4,6-TNP, 0.05 M Na₂SO₄ + 0.01 M NaCl, pH 4, scan rate: 50 mV s⁻¹.

compounds in solutions, causing the diminishing of adsorbed hydroxyl radicals on the surface of PbO₂. The removal of hydroxyl radicals from the active centers promotes reactions (5) and (6). The promotion of these reactions would accelerate the transfer of electrons in the zone of gel-crystal which resulted in the increase of current, resulting in the observed increase in oxidation current shown in Fig. 4. In addition, the slight increase of potential would not result in the significant increase of current in CVs. In previous study, Compton and his co-workers also attribute the increase of current to the consumption of hydroxyl radicals [48]. Therefore, the increase of current in CVs was mainly due to the promoted reactions (5) and (6).

3.3. Bulk electrolysis

The variation of COD removals of 2,4-DNP, 2,5-DNP, 2,6-DNP and 2,4,6-TNP are presented in Fig. 5(a–d), respectively. In this figure, it can be seen that the degrees of removal of all NPs exceeded 90% when electrolysis time reached 120 min. The removal rate of 2,6-DNP was faster than the three other NPs, which indicated that this compound could be electrochemically oxidized more easily than 2,4-DNP, 2,5-DNP and 2,4,6-TNP. In previous researches [24,34,35], the electrocatalytic oxidation of phenolic compounds would lead to the formation of carboxylic acids, which were more difficult to be decomposed than phenolic compounds. The fast removal of COD observed in the beginning

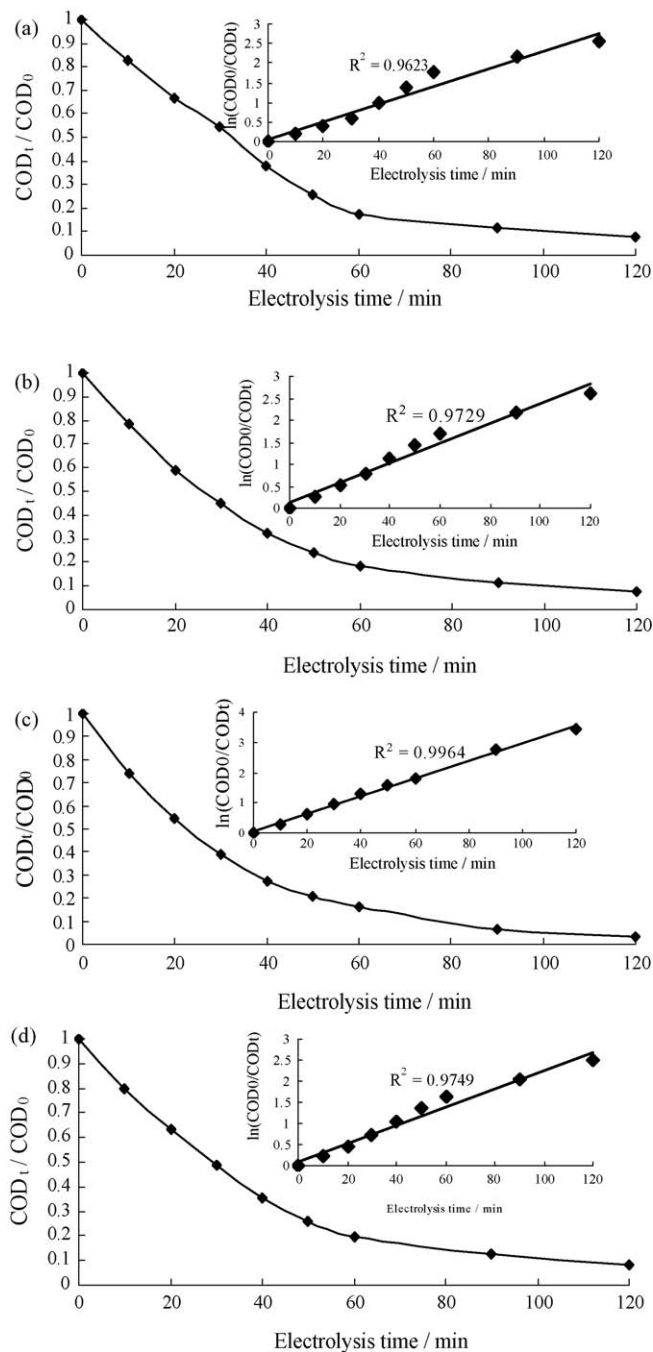


Fig. 5. Trend of normalized COD as a function of electrolysis time in the electrochemical oxidation of NPs: (a) 2,4-DNP; (b) 2,5-DNP; (c) 2,6-DNP and (d) 2,4,6-TNP, inset: $\ln(\text{COD}_0/\text{COD}_t)$.

could be attributed to the rapid degradation of aromatic compounds, while the final slowing down reflected a much slower mineralization of carboxylic acids originated by ring fission. As shown in the insets of Fig. 5, all the correlation coefficients about the $\ln(\text{COD}_0/\text{COD}_t)$ vs t for the four NPs were more than 9.6. Therefore, the variation of COD could be considered as typical exponential shapes for all NPs, which illustrated that the electrocatalytic oxidation processes of NPs were mass-transfer controlled [35]. The same phenomena were observed in our previous researches for mono-substituted nitrophenols as well [24]. Therefore, it can be inferred that the present electrochemical system consisted of Bi-doped lead dioxide anode is favorable to mass-transfer of organic compounds.

Fig. 6 shows the evolution with electrolysis time of the normalized NPs. It can be seen that the concentration of NPs decreased progressively as the electrolysis time proceeded, leading to complete elimination of 2,6-DNP and almost total decomposition of 2,5-DNP and 2,4-TNP. However, at the end of electrolysis, small portion of 2,4,6-TNP still existed in solution. This diagram also demonstrated a faster degradation velocity of 2,6-DNP, followed by 2,5-DNP, 2,4-TNP and 2,4,6-TNP. The regression analysis of the concentration curves vs reaction time indicated that the decomposition rate of these NPs could also be described by the pseudo-first-order kinetics formula with respect to NP concentration: $dC_{\text{NP}}/dt = -kC_{\text{NP}}$. Though NPs would react with oxidants such as hydroxyl radicals, the concentrations of these oxidants were constant and larger than those of NPs. Therefore, the kinetics models could be simplified as pseudo-first-order, in which the evolution of concentration of NPs was the only variable. The value of pseudo-first-order rate constants k of three NPs were calculated and listed in Table 1, as well as the correlation coefficients. The results suggested that the degradation of NPs lies in the order: 2,6-DNP > 2,5-DNP > 2,4-DNP > 2,4,6-TNP.

In previous studies, nitro group has been testified to have effect on properties of NPs in terms of its position on aromatic ring [24,49]. The Hammett constant represents the effect that the various substituents have on the electronic character of a given aromatic system [50]. Hammett constant (σ) of multi-substituted nitrophenol (shown in Table 1) was calculated as a sum of σ 's of nitro groups, adopting the values 0.71, 0.78 and 1.24, respectively, for *meta*-, *para*- and *ortho*-positions [51]. The larger value corresponded to stronger electron-withdrawing capacity of groups. Some researchers concluded that the degradation phenolic compounds followed the law of Hammett constant, i.e., the degradation rate had a linear relationship with the value of Hammett constant. Ksibi et al. [14] reported their investigation on the relationship between Hammett constant and the degradation of three kinds of NPs with different number of nitro group on aromatic rings. They pointed out that the smaller the Hammett constant was, the faster the compounds were decomposed. In other words, the more the number of substituent was, the more difficult it could be oxidized. Zhu et al. [49] also studied the relationship between Hammett constant and the nature of *p*-

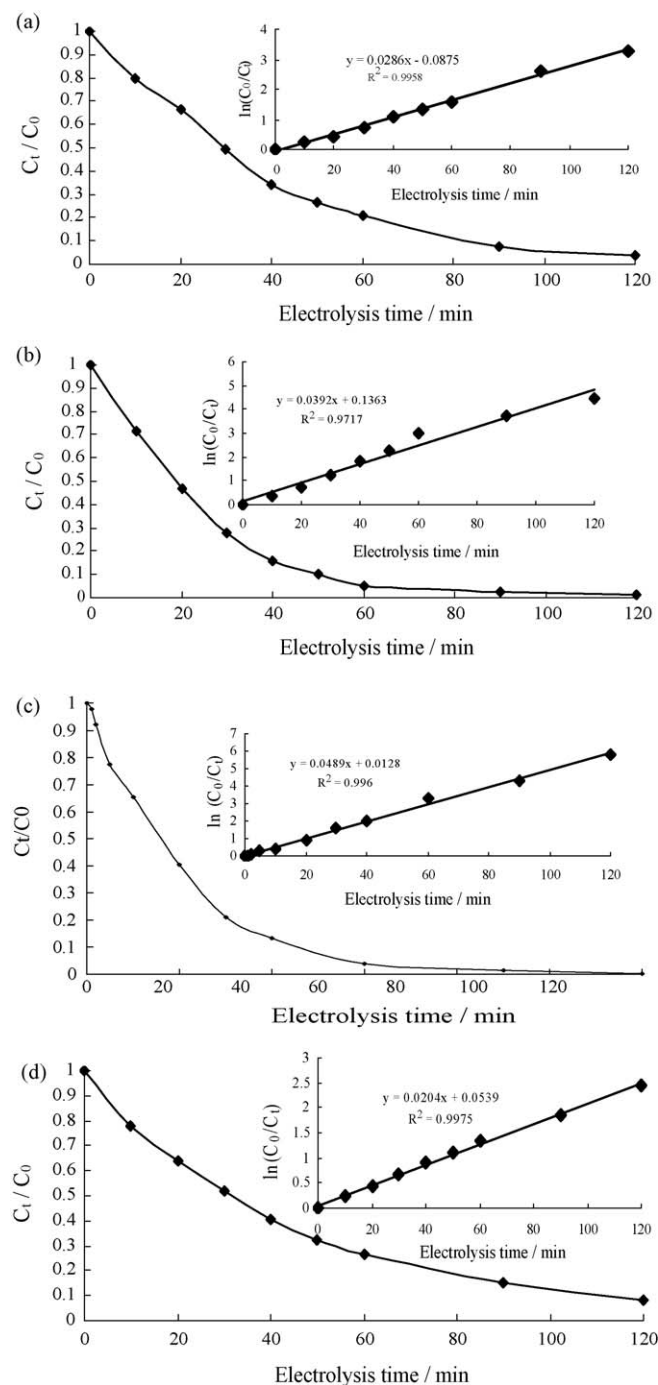


Fig. 6. Trend of normalized NP concentration as a function of electrolysis time in the electrochemical oxidation of NPs: (a) 2,4-DNP; (b) 2,5-DNP; (c) 2,6-DNP and (d) 2,4,6-TNP, inset: $\ln(C_0/C_t)$.

Table 1
Pseudo-first-order rate constants k of NPs as well as their Hammett constants (σ) and melting point (T_{fus}).

| NPs | k (min^{-1}) | Correlation coefficient R^2 | σ | T_{fus} (K) |
|---------------------------|---------------------------|-------------------------------|----------|----------------------|
| <i>o</i> -NP ^a | 0.0988 | 0.9723 | 1.24 | 318.4 |
| <i>m</i> -NP ^a | 0.0709 | 0.9750 | 0.71 | 370.5 |
| <i>p</i> -NP ^a | 0.0513 | 0.9157 | 0.78 | 387.3 |
| 2,4-DNP | 0.0286 | 0.9958 | 2.02 | 386 |
| 2,5-DNP | 0.0392 | 0.9717 | 1.95 | 379 |
| 2,6-DNP | 0.0489 | 0.9960 | 2.48 | 336.5 |
| 2,4,6-TNP | 0.0204 | 0.9975 | 3.26 | 394.8 |

^a Data from ref. [24].

substituted phenols with different kinds of substituents. They came out an opposite conclusion that the degradation rate of *p*-substituted phenols rose with an increase of Hammett constants. However, neither of the two conclusions was in agreement with the present results. Despite the highest Hammett constant among dinitrophenols, the degradation rate of 2,6-DNP was also the fastest. The similar result has been reported in our previous study as well [24]. In that work, we investigated the electrocatalytic oxidation of three kinds of mono-substituted nitrophenol. *o*-Nitrophenol, with the highest Hammett constant, was more readily electrochemically oxidized than *m*-nitrophenol and *p*-nitrophenol. On the other hand, combining the two parts of results,

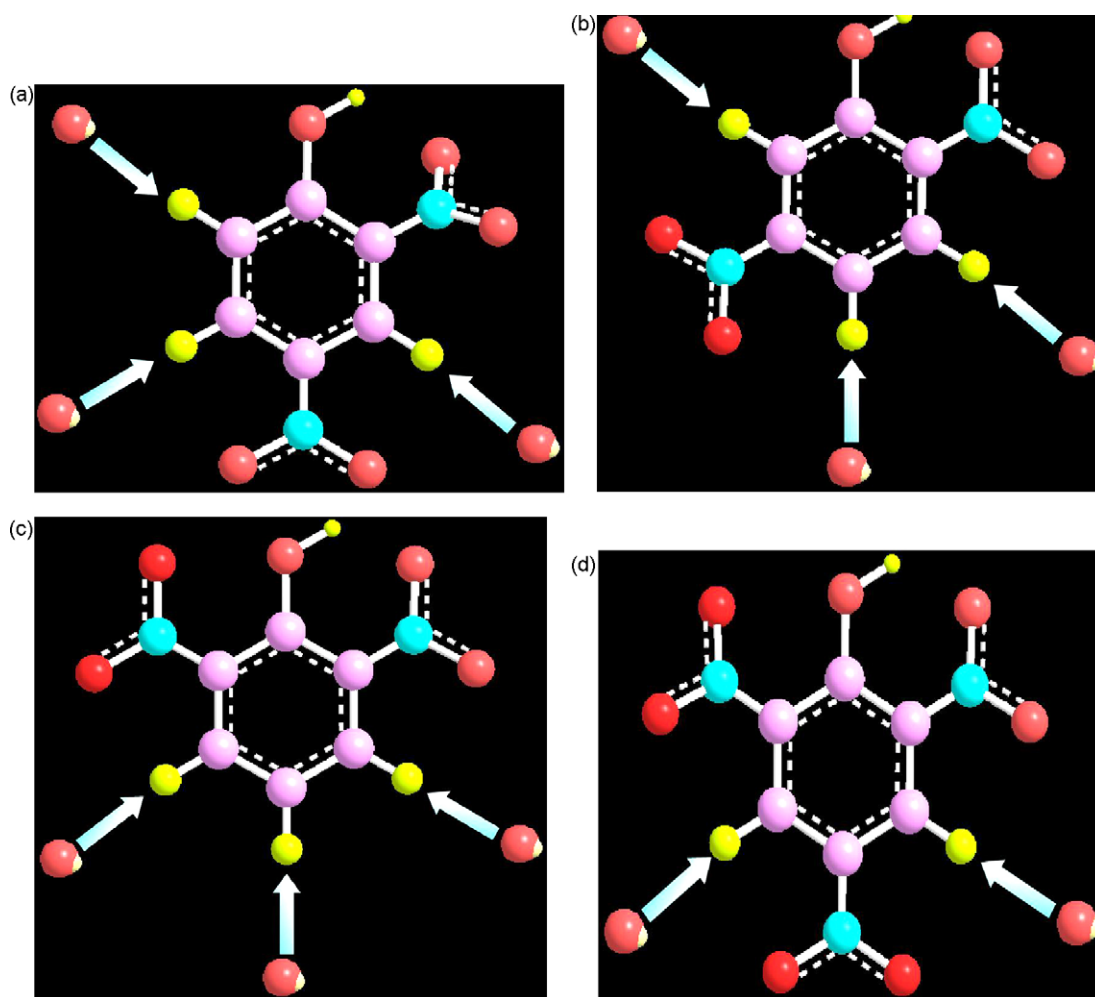


Fig. 7. Scheme of reaction between hydroxyl radicals and nitrophenol molecules: (a) 2,4-DNP; (b) 2,5-DNP; (c) 2,6-DNP and (d) 2,4,6-TNP, the balls represent hydroxyl radical.

it could be seen that the degradation rates of dinitrophenol were all smaller than those of mono-nitrophenol. In addition, the degradation rate of 2,4,6-TNP was smaller than any kind of dinitrophenol as shown in Table 1. At this point, the degradation of nitrophenols conformed to the law of Hammett constant. Therefore, we could infer that the law of Hammett constant was more suitable for the degradation of phenolic compounds which contained different number of substituents or different kinds of substituents, but not for those phenolic compounds which contained the same number and same kind of substituent. With regarding to NPs, the degradation rates of these compounds lie in the following order: mono- > di- > tri-NP.

Hydroxyl radical has a strong electrophilic character, and attacks those groups or carbon atom of the aromatic ring with high electron density preferentially. The attack of electrophilic hydroxyl radicals occurs at ring position activated by the presence of two substituents in NPs, namely hydroxyl (–OH) and nitro (–NO₂) group. The electron-donating substituent, phenolic –OH group, increase the electron density at *ortho* and *para* positions, while electron-withdrawing substituent, –NO₂ group, is strongly deactivating the *meta* position. When both these substituents (–OH and –NO₂) are present, the electrophilic attack will occur preferentially in *ortho* and *para* positions with respect to phenolic –OH group. Taking into account of the structure of the three dinitrophenols, 2,6-DNP displayed an open structure at the *para* position. When hydroxyl radicals attacked this position, it would encounter the smallest resistance from other groups (–OH and –NO₂). Therefore,

it was the most easily for 2,6-DNP to be electrocatalytic oxidized. On the other hand, when hydroxyl radicals attacked aromatic rings of 2,4-DNP and 2,5-DNP, it would become tough owing to the steric effects of the second –NO₂ group at the *para* and *meta* position on aromatic rings, respectively. As for the molecular structure of 2,4,6-TNP, it has the largest steric resistance. The scheme of reactions between hydroxyl radicals and nitrophenol molecules are demonstrated in Fig. 7. It can be seen from this figure that the attacking of hydroxyl radicals to aromatic ring of 2,6-DNP seemed to be the most readily. As a consequence, it could be inferred that the structure of a compound would influence its decomposition in some extent.

Besides the electron-withdrawing effect of –NO₂ group, hydrogen bonds play an important role in the process of electrocatalytic oxidation of NPs as well. From Table 1, one can see that the melting point (T_{fus}) [52] of 2,6-DNP was the smallest among the three isomers of dinitrophenols. Moreover, the order of melting points was consistent of that of degradation rate as long as the same number of nitro group on aromatic ring. It was due to the reason that the value of T_{fus} was concerned with the molecular structures of these compounds. There are intermolecular and intramolecular hydrogen bonds thanks to the existence of –OH group [53]. The different strength of these hydrogen bonds leads to the different physicochemical characteristics of NP isomers. The distinct values of T_{fus} of NP isomers reflect the different stability of these NPs. As a result, the T_{fus} also indicates that it is much more ready to eliminate 2,6-DNP.

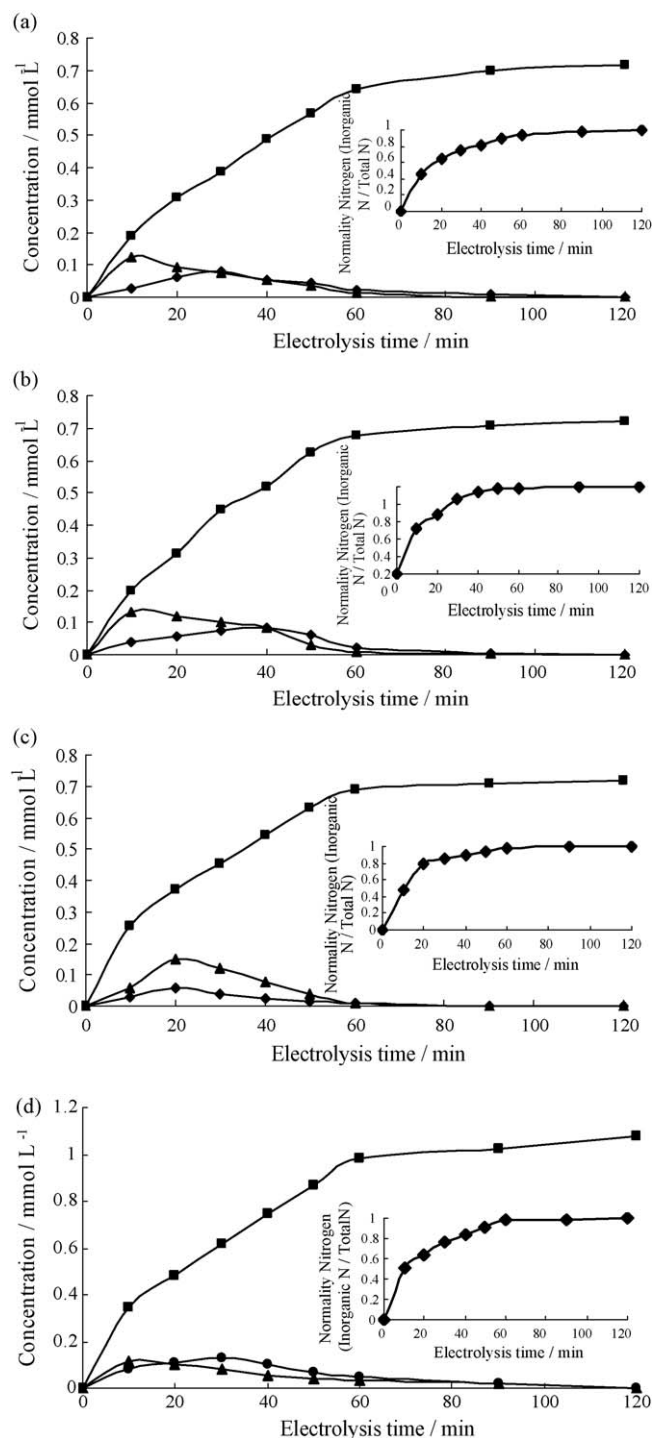


Fig. 8. Time evolution of nitrate and ammonia ions in the electrochemical degradation of (a) 2,4-DNP, (b) 2,5-DNP and (c) 2,4,6-TNP (■) NO_3^- , (□) NO_2^- , (▲) NH_4^+ , inset: variation of the ratio of inorganic nitrogen to total nitrogen as a function of electrolysis time.

The kinetics of NO_3^- , NO_2^- and NH_4^+ are given in Fig. 8(a–d) for 2,4-DNP, 2,5-DNP, 2,6-DNP and 2,4,6-TNP, respectively. From the figure, one can see that only a small amount of NO_2^- and NH_4^+ formed and accumulated in solutions in the course of 2-h electrolysis. According to the insets, the ratio of inorganic nitrogen to total nitrogen was approximately equal to 1 at the end of each run of electrolysis, indicating that almost all of the nitro groups were eliminated from aromatic rings. The ratio of inorganic nitrogen to total nitrogen was calculated by the

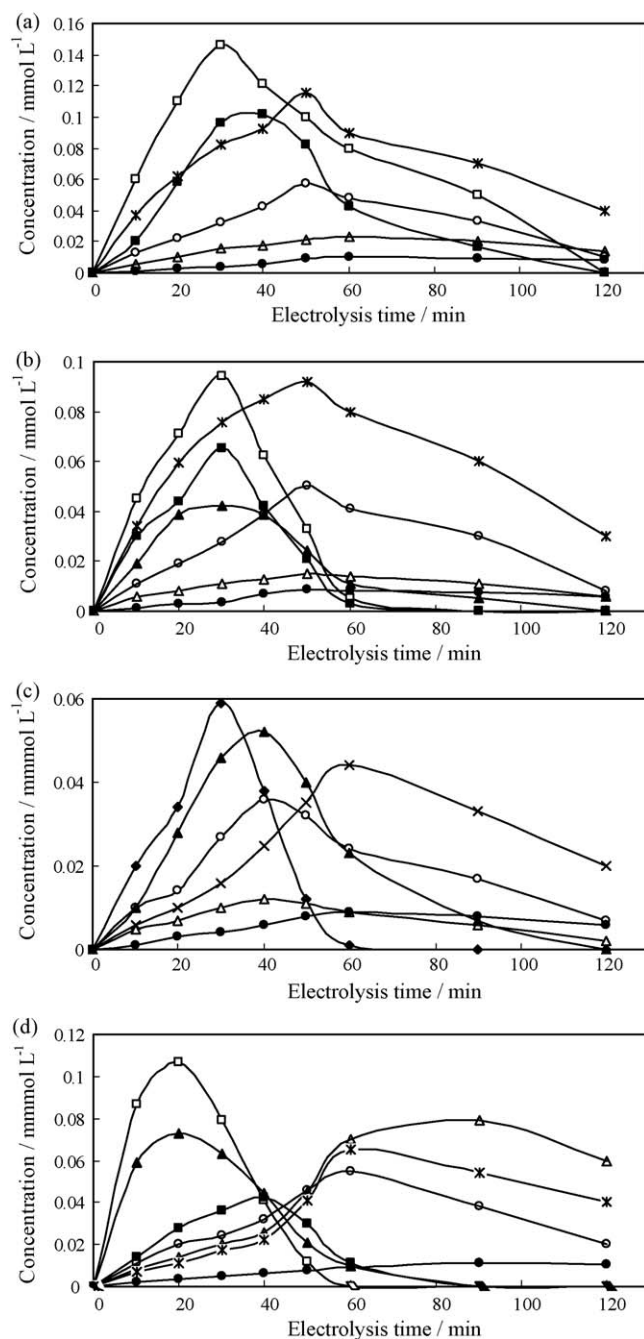


Fig. 9. Variation of concentration of intermediates as a function of electrolysis time, (a) 2,4-DNP: (□) *p*-nitrophenol; (■) Benzoquinone; (○) maleic acid; (△) malonic acid; (*) oxalic acid; (●) acetic acid. (b) 2,5-DNP: (□) *m*-nitrophenol; (■) *o*-nitrophenol; (▲) catechol; (○) maleic acid; (□) malonic acid; (*) oxalic acid; (●) acetic acid. (c) 2,6-DNP: (◆) *o*-nitrophenol; (▲) catechol; (○) maleic acid; (△) malonic acid; (*) oxalic acid; (●) acetic acid. (d) 2,4,6-TNP: (□) 2,4-dinitrophenol; (■) *p*-nitrophenol; (▲) *o*-nitrophenol; (○) maleic acid; (△) malonic acid; (*) oxalic acid; (●) acetic acid.

formula: $C_{\text{NO}_3^-} + C_{\text{NO}_2^-} + C_{\text{NH}_4^+} / n \times C_{\text{NP}}$, where, $C_{\text{NO}_3^-}$, $C_{\text{NO}_2^-}$, $C_{\text{NH}_4^+}$ were the concentration of and NO_3^- , NO_2^- and NH_4^+ (mmol L^{-1}), respectively, C_{NP} was the initial concentration of NPs (mmol L^{-1}), n was number of nitro group of NPs. This ratio could be used as the index which indicated what the extent of nitro group detached from aromatic ring. The formation of ammonia ions was attributed to the reduction of nitrate at the cathode. At the end of electrolysis, nitro groups were all converted to NO_3^- .

3.4. Proposed mechanism

In order to propose a tentative degradation pathway of these NPs, it is essential to detect the intermediates and their evolution as the electrolysis proceeded. LC/MS and HPLC were used to monitor the intermediates and generated during the oxidation processes qualitatively and quantitatively, respectively. The results of LC/MS and HPLC for 2,4-DNP, 2,5-DNP, 2,6-DNP and 2,4,6-TNP are presented in Tables 2–5 and Fig. 9(a–d), respectively.

Table 2
Observed ions and possible compounds for analysis of LC/MS of 2,4-DNP.

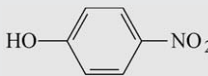
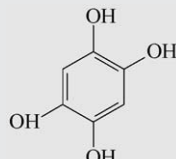
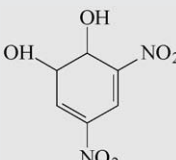
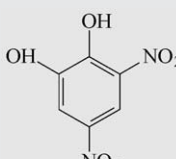
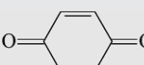
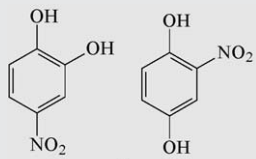
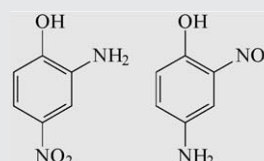
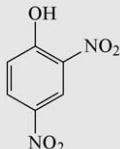
| m/z | Ion assignment | Compound |
|----------------------|--------------------------------|---|
| Positive mode | | |
| 87 | $[M+H]^+$ | $H_2C=CH-CH_2-COOH$ |
| 105 | $[M+H]^+$ | $HOOC-CH_2-COOH$ |
| 117 | $[M+H]^+$ | $HOOC-CH=COOH$ |
| 131 | $[M+H]^+$ | $HOOC-CH_2-CH=CH-COOH$ |
| 140 | $[M+H]^+$ |  |
| 165 | $[M+Na]^+$ |  |
| 199 | $[M+H]^+$ |  |
| 201 | $[M+H]^+$ |  |
| Negative mode | | |
| 97 | $[M+HCOO^-+HCOO^-]^{2-}$ | $HOOC-CH_2-COOH$ |
| 99 | $[M+HCOO^-+HCOO^-]^{2-}$ |  |
| 115 | $[M-H]^-$ | $HOOC-CH=CH-COOH$ |
| 137 | $[M+CH_3COO^-+CH_3COO^-]^{2-}$ |  |

Table 2 (Continued)

| m/z | Ion assignment | Compound |
|-----|----------------|---|
| 153 | $[M-H]^-$ |  |
| 165 | $[M+HCOO^-]^-$ | $HOOC-CH(OH)-COOH$ |
| 183 | $[M-H]^-$ |  |

It can be seen from Tables 2–5 that three kinds of intermediates were detected, i.e., polyhydroxylated intermediates, reduction products of NPs and carboxylic acids. With respect to the formation of polyhydroxylated intermediates, the most possible reason is as follows. The attack of hydroxyl radicals belongs to electrophilic attack, so that the reaction took place preferentially at those positions with higher electron density. If the position was occupied by a nitro group, the denitration from aromatic rings occurred. If the position were vacant, the addition of hydroxyl group to the benzene ring would result in the formation of polyhydroxylated intermediates. On the other hand, the substitution of nitro group and hydrogen atom on the aromatic rings by hydroxyl radical also took place. Some researchers considered the addition of hydroxyl group to aromatic rings was a dominating reaction in the first part of degradation [8,54]. However, in our opinion, whether denitration or addition of hydroxyl group happened in the first part of degradation was dependent on the structure of organic compounds. In the present work, the denitration and substitution by hydroxyl radicals on aromatic rings seem to be the first stage. The polyhydroxylation would subsequently lead to the opening of aromatic rings to form variety of carboxylic acids. However, considering the discrepancy between concentration of denitrated aromatic compounds or carboxylic acids detected and that of nitrate formed (Figs. 8 and 9), there might be another pathway in which the opening of aromatic rings took place before nitro group was substituted and nitrated aliphatic compounds was formed (see in Table 4).

In addition, some reduction products of NPs were also detected in the present study. Aminophenols (APs) were detected in terms of the results of LC–MS during the electrolysis of 2,4-DNP, 2,5-DNP and 2,4,6-TNP. In our previous study [24], GC/MS found the existence of APs as well. This phenomenon indicated that the reduction of NPs to APs took place at the cathode. Then, these APs disappeared gradually with the electrolysis went on. Previous researches [55,56] reported that APs would be polymerized to transform into a dark brown solid that remained on the surface of cathode up to the end of treatment. However, this dark brown solid was not observed in all of our experimental runs. It can be inferred that these APs were completely oxidized ultimately under the present experimental conditions.

Organic acids were formed as a result of the opening of aromatic rings. Some researchers pointed out that other highly hydrophilic compounds such as ethane, aldehyde, ketone and other carbonyl compounds were also detected which could be expected as in the

Table 3

Observed ions and possible compounds for analysis of LC/MS of 2,5-DNP.

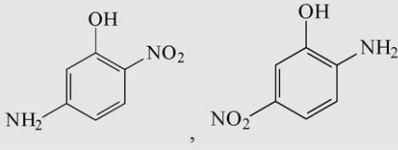
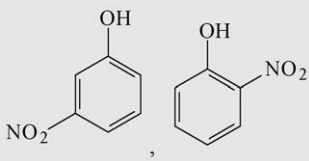
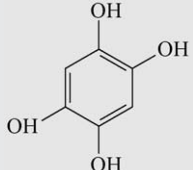
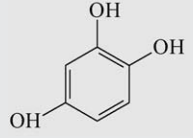
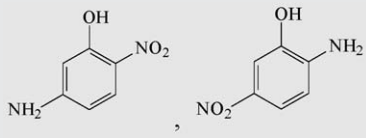
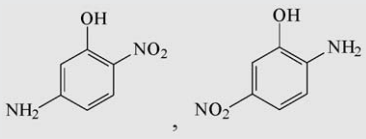
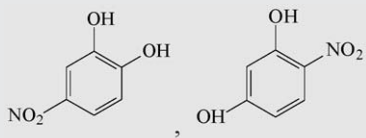
| <i>m/z</i> | Ion assignment | Compound |
|---------------|----------------------------------|---|
| Positive mode | | |
| 87 | $[M+H]^+$ | $H_2C=CH-CH_2-COOH$ |
| 105 | $[M+H]^+$ | $HOOC-CH_2-COOH$ |
| 119 | $[M+H]^+$ | $HOOC-CH_2-CH_2-COOH$ |
| 123 | $[M+Na]^+$ | $H_2C=CH-CH_2-CH_2-COOH$ |
| 155 | $[M+H]^+$ |  |
| 162 | $[M+Na]^+$ |  |
| 165 | $[M+Na]^+$ |  |
| 175 | $[M+Na+Na-H]^+$ | $HOOC-CH_2-CH=CH-COOH$ |
| Negative mode | | |
| 80 | $[M+HCOO^- - H]^{2-}$ | $HOOC-CH=CH-COOH$ |
| 97 | $[M+HCOO^- + HCOO^-]^{2-}$ | $HOOC-CH_2-COOH$ |
| 125 | $[M-H]^-$ |  |
| 136 | $[M+CH_3COO^- + CH_3COO^-]^{2-}$ |  |
| 153 | $[M+HCOO^-]^-$ |  |
| 154 | $[M-H]^-$ |  |

Table 3 (Continued)


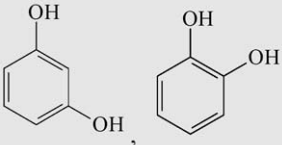
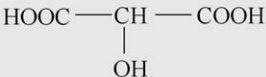
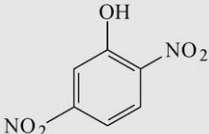
| <i>m/z</i> | Ion assignment | Compound |
|------------|-----------------|---|
| 155 | $[M+CH_3COO]^-$ |  |
| 155 | $[M+HCOO]^-$ |  |
| 179 | $[M+CH_3COO]^-$ |  |
| 183 | $[M-H]^-$ |  |

Table 4

Observed ions and possible compounds for analysis of LC/MS of 2,6-DNP.

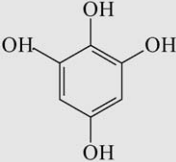
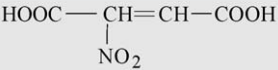
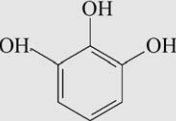
| <i>m/z</i> | Ion assignment | Compound |
|----------------------|--------------------------------|---|
| Positive mode | | |
| 87 | $[M+H]^+$ | $H_2C=CH-CH_2-COOH$ |
| 105 | $[M+H]^+$ | $HOOC-CH_2-COOH$ |
| 119 | $[M+H]^+$ | $HOOC-CH_2-CH_2-COOH$ |
| 165 | $[M+Na]^+$ |  |
| 184 | $[M+Na]^+$ |  |
| Negative mode | | |
| 89 | $[M+CH_3COO^-+CH_3COO^-]^{2-}$ | CH_3COOH |
| 97 | $[M+HCOO^-+HCOO^-]^{2-}$ | $HOOC-CH_2-COOH$ |
| 117 | $[M-H]^-$ | $HOOC-CH_2-CH_2-COOH$ |
| 125 | $[M-H]^-$ |  |
| 129 | $[M-H]^-$ | $HOOC-CH_2-CH=CH-COOH$ |

Table 4 (Continued)

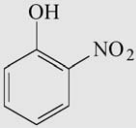
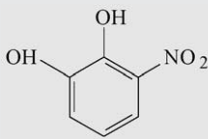
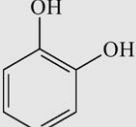
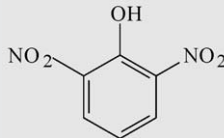
| m/z | Ion assignment | Compound |
|-----|-------------------------------|--|
| 138 | $[M-H]^-$ |  |
| 148 | $[M-H]^-$ | $\text{HOOC}-\underset{\text{NO}_2}{\text{CH}_2}-\text{COOH}$ |
| 154 | $[M-H]^-$ |  |
| 169 | $[M+\text{CH}_3\text{COO}]^-$ |  |
| 179 | $[M+\text{CH}_3\text{COO}]^-$ | $\text{HOOC}-\underset{\text{OH}}{\text{CH}}-\text{COOH}$ |
| 183 | $[M-H]^-$ |  |
| 222 | $[M+\text{CH}_3\text{COO}]^-$ | $\text{HOOC}-\underset{\text{NO}_2}{\text{CH}}-\text{CH}_2-\text{COOH}$ |

Table 5

Observed ions and possible compounds for analysis of LC/MS of 2,4,6-TNP.

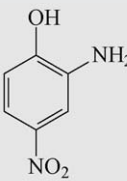
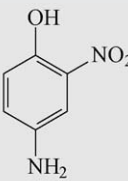
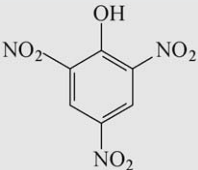
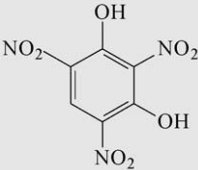
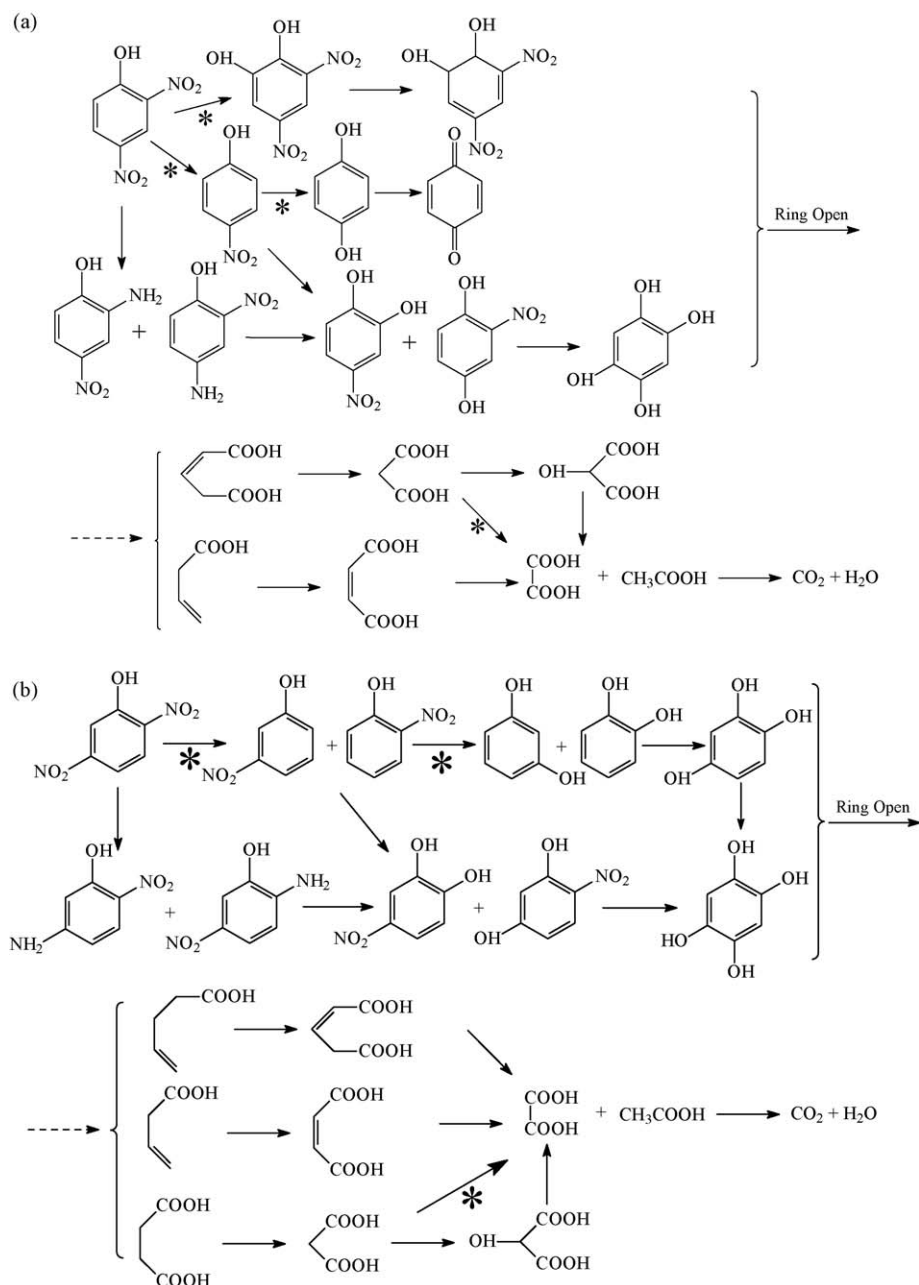
| m/z | Ion assignment | Compound |
|---------------|-------------------|---|
| Positive mode | | |
| 87 | $[M+H]^+$ | $\text{H}_2\text{C}=\text{CH}-\text{CH}_2-\text{COOH}$ |
| 105 | $[M+H]^+$ | $\text{HOOC}-\text{CH}_2-\text{COOH}$ |
| 119 | $[M+H]^+$ | $\text{HOOC}-\text{CH}_2-\text{CH}_2-\text{COOH}$ |
| 123 | $[M+\text{Na}]^+$ | $\text{H}_2\text{C}=\text{CH}-\text{CH}_2-\text{CH}_2-\text{COOH}$ |
| 139 | $[M+\text{Na}]^+$ | $\text{HOOC}-\text{CH}=\text{CH}-\text{COOH}$ |
| 155 | $[M+H]^+$ |   |

Table 5 (Continued)

| <i>m/z</i> | Ion assignment | Compound |
|---------------------|---|--|
| 165 | [M+Na] ⁺ | |
| 175 | [M+Na+Na-H] ⁺ | HOOC-CH ₂ -CH=CH-COOH |
| 207 | [M+Na] ⁺ | |
| 223 | [M+Na] ⁺ | |
| Negative mode 97 | [M+HCOO ⁻ +HCOO ⁻] ²⁻ | HOOC-CH ₂ -COOH |
| 99 | [M-H] ⁻ | H ₂ C=CH-CH ₂ -CH ₂ -COOH |
| 141 | [M-H] ⁻ | |
| 165 | [M+HCOO ⁻] ⁻ | |
| 183 | [M-H] ⁻ | |
| 199 | [M-H] ⁻ | |
| 217 | [M+CH ₃ COO] ⁻ | |

Table 5 (Continued)

| m/z | Ion assignment | Compound |
|-----|----------------|---|
| 228 | $[M-H]^-$ |  |
| 246 | $[M-H]^-$ |  |

Fig. 10. Possible degradation pathway of NPs on Bi-doped PbO₂ electrode: (a) 2,4-DNP; (b) 2,5-DNP; (c) 2,6-DNP and (d) 2,4,6-TNP, (*) represents the major reactions.

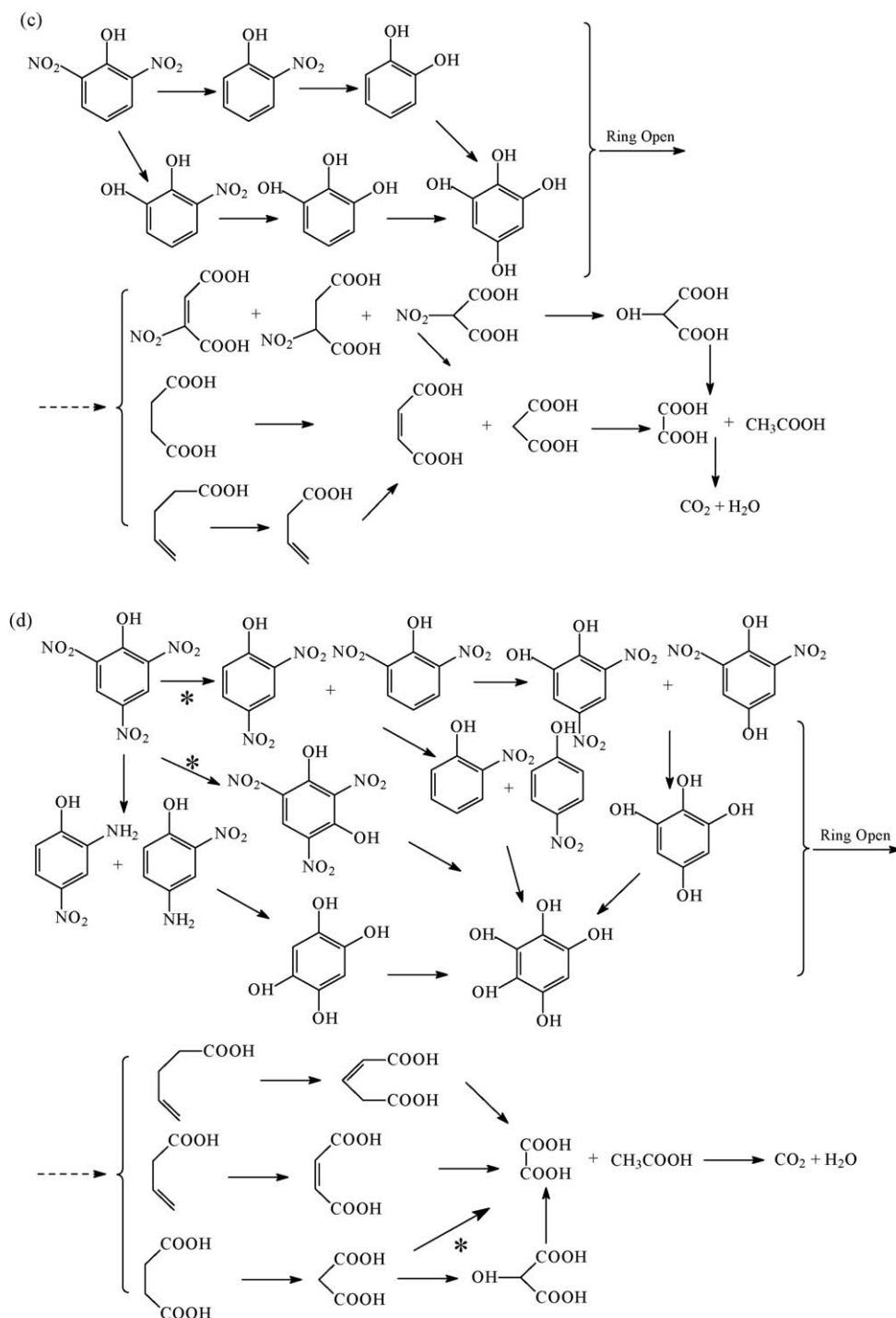


Fig. 10. (Continued).

case of other oxidative degradation [57,58]. In this study, these compounds were not detected by LC/MS or HPLC. Among organic acids detected, oxalic and acetic acids are largest in concentration, as shown in Fig. 9. As a matter of fact, a spot of maleic acid and malonic acid still remained in solutions as well as oxalic acid and acetic acid, which proved that carboxylic acids were more difficult to be oxidized by hydroxyl radicals than aromatic compounds [34,59,60]. In addition, formic acid was not detected in this work, which might be ascribed to the reason that formic acid was much more degradable than acetic acid. Hence, it could be considered that most portions of dinitrophenols eventually converted to carbon dioxide via formic acid.

Finally, either polyhydroxylated intermediates or carboxylic acids were oxidized into CO_2 and H_2O . According to the above mentioned results, possible degradation pathways of 2,4-DNP, 2,5-DNP, 2,6-DNP and 2,4,6-TNP were proposed as shown in Fig. 10(a–d), respectively.

4. Conclusions

Titanium based Bi-doped lead dioxide anode displays porous structure with small-sized crystal particles and a very compact crystalline structure. Oxidants, such as hydroxyl radical, hydrogen peroxide and hypochlorite ion were detected in the

present electrochemical system. The results of CVs indicate that direct oxidation of nitrophenols on surface of Bi-doped lead dioxide electrode does not play an important role. Moreover, there are no polymeric adhesive compounds formed and deposited on the surface of electrode in the present work. Electrochemical oxidation using Bi-doped lead dioxide anode can be successfully used for the treatment of aqueous nitrophenol wastes. The profiles of COD variation illustrate that the electrochemical oxidation processes of NPs are mass-transfer controlled. The electrochemical oxidation processes of NPs can be modeled as pseudo-first-order kinetics. The value of pseudo-first-order rate constants of these NPs demonstrates the oxidation of them lies in the order: 2,6-DNP > 2,5-DNP > 2,4-DNP > 2,4,6-TNP. The results reveal that the structures of NPs significantly influence the electrochemical oxidation of NPs. The dependence of degradation rate on the number of nitro group reveals that on one hand, the more the number of nitro group is, the less the degradation rate is. On the other hand, with the same number of nitro group, the order of degradation rate is in agreement with that of melting point of nitrophenol. The results of LC/MS and HPLC suggest that three kinds of intermediates are generated, i.e., polyhydroxylated intermediates, reduction products of NPs and carboxylic acids. The degradation pathway of nitrophenol can be depicted as follows. The denitration and substitution by hydroxyl radicals on aromatic rings seem to be the first stage. As a consequence, the formation of *o*-nitrophenol, *p*-nitrophenol and *m*-nitrophenol takes place, as well as some polyhydroxylated intermediates. These compounds are successively oxidized into catechol, resorcinol and hydroquinone, followed by the opening of aromatic rings and the formation of a series of carboxylic acids. Finally, these carboxylic acids are oxidized into CO₂ and H₂O.

Acknowledgement

This work was supported by National Creative Research Groups, National Natural Science Foundation of China (no. 50821002).

Appendix A. Supplementary data

Supplementary data associated with this article can be found, in the online version, at doi:10.1016/j.apcatb.2009.05.039.

References

- [1] R. Belloli, E. Bolzacchini, L. Clerici, B. Rindone, G. Sesana, V. Librando, *Environ. Eng. Sci.* 23 (2006) 405–415.
- [2] USEPA, Health and environmental effects profile for nitrophenols [S], Environmental Protection Agency, Environmental Criteria and Assessment Office, Cincinnati, OH, US, 1985.
- [3] M. Shimazu, A. Mulchandani, W. Chen, *Biotechnol. Bioeng.* 76 (2001) 318–324.
- [4] J.B. Lippincot, List of Worldwide Hazardous Chemical and Pollutants, The Forum for Scientific Excellence, New York, 1990.
- [5] M.S. Dieckmann, K.A. Gray, *Water. Res.* 30 (1996) 1169–1183.
- [6] J. Kiwi, C. Pulgarin, C. Peringer, *Appl. Catal. B: Environ.* 3 (1994) 335–350.
- [7] A. Gutes, F. Cespedes, S. Alegret, M. Del Valle, *Biosens. Bioelectron.* 20 (2005) 1668–1673.
- [8] K. Tanaka, W. Luesaiwong, T. Hisanaga, *J. Mol. Catal. A: Chem.* 122 (1999) 67–74.
- [9] K.W. Hofmann, H.J. Knackmuss, G. Heiss, *Appl. Environ. Microb.* 70 (2004) 2854–2860.
- [10] Z. Aleksieva, D. Ivanova, T. Godjevargova, B. Atanasov, *Process. Biochem.* 37 (2002) 1215–1219.
- [11] S. Yi, W.Q. Zhuang, B. Wu, S.T.L. Tay, J.H. Tay, *Environ. Sci. Technol.* 40 (2006) 2396–2401.
- [12] M.C. Tomei, M.C. Annesini, R. Luberti, G. Cento, A. Senia, *Water. Res.* 37 (2003) 3803–3814.
- [13] V.L. Geminia, A. Gallegoa, V. Tripodib, D. Corach, E.I. Planesc, S.E. Korol, *Int. Biodeterior. Biodegrad.* 60 (2007) 226–230.
- [14] M. Ksibi, A. Zemzemi, R. Boukchina, *J. Photochem. Photobiol. A: Chem.* 159 (2003) 61–70.
- [15] V. Kavitha, K. Palanivelu, *J. Photochem. Photobiol. A: Chem.* 170 (2005) 83–95.
- [16] A. Goi, M. Trapido, *Chemosphere* 46 (2002) 913–922.
- [17] A. Goi, M. Trapido, T.A. Tuhkanen, *Adv. Environ. Res.* 8 (2004) 303–311.
- [18] M.E. Makgae, M.J. Klink, A.M. Crouch, *Appl. Catal. B: Environ.* 84 (2008) 659–666.
- [19] Z.H. Teng, Y.J. Wang, B. Wu, Y.W. Tang, T.H. Lu, Y. Gao, *Appl. Catal. B: Environ.* 84 (2008) 400–407.
- [20] F. Harnisch, U. Schröder, M. Quaa, S. Scholz, *Appl. Catal. B: Environ.* 84 (2008) 63–69.
- [21] K. Rajeshwar, J.G. Ibanez, *Environmental Electrochemistry: Fundamentals and Applications in Pollution Abatement*, Academic Press, San Diego, CA, 1997.
- [22] M.A. Quiroz, S. Reyna, C.A. Martínez-Huitle, S. Ferro, A. De Battisti, *Appl. Catal. B: Environ.* 59 (2005) 259–266.
- [23] M. Panizza, G. Cerisola, *Appl. Catal. B: Environ.* 75 (2007) 95–101.
- [24] Y. Liu, H.L. Liu, Y. Li, *Appl. Catal. B: Environ.* 84 (2008) 297–302.
- [25] D.C. Johnson, J. Feng, L.L. Houk, *Electrochim. Acta* 46 (2000) 323–330.
- [26] M.H. Zhou, Q.Z. Dai, L.C. Lei, C.A. Ma, D.H. Wang, *Environ. Sci. Technol.* 39 (2005) 363–370.
- [27] Ch. Comninellis, *Electrochim. Acta* 39 (1994) 1857–1862.
- [28] K.L. Pamplin, D.C. Johnson, *J. Electrochem. Soc.* 143 (1996) 2119–2125.
- [29] N.B. Tahar, A. Savall, *J. Appl. Electrochem.* 29 (1999) 277–283.
- [30] N.D. Popović, J.A. Cox, D.C. Johnson, *J. Electrochem. Chem.* 456 (1998) 203–209.
- [31] H.L. Liu, Y. Liu, C. Zhang, R.S. Shen, *J. Appl. Electrochem.* 38 (2008) 101–108.
- [32] Y. Liu, H.L. Liu, *Electrochim. Acta* 53 (2008) 5077–5083.
- [33] P. Cañizares, C. Sáez, J. Lobato, M.A. Rodrigo, *Electrochim. Acta* 49 (2004) 4641–4650.
- [34] P. Cañizares, J. Lobato, R. Paz, M.A. Rodrigo, C. Sáez, *Water. Res.* 39 (2005) 2687–2703.
- [35] B. Nasr, G. Abdellatif, *J. Electrochem. Soc.* 152 (2005) D113–D116.
- [36] B. Tang, L. Zhang, Y. Geng, *Talanta* 65 (2005) 769–775.
- [37] F.J. Welcher, 6th ed., Standard methods of chemical analysis, part B, vol. 2, R.E. Krieger Publishing Co Huntington, New York, 1975, p. 1827.
- [38] C. Carlesi-Jara, D. Fino, V. Specchia, G. Saracco, P. Spinelli, *Appl. Catal. B Environ.* 70 (2007) 479–487.
- [39] Ch. Comninellis, C. Pulgarin, *J. Appl. Electrochem.* 21 (1991) 703–708.
- [40] Ch. Comninellis, C. Pulgarin, *J. Appl. Electrochem.* 23 (1993) 108–112.
- [41] G.R.P. Malpass, D.W. Miwa, D.A. Mortari, S.A.S. Machado, A.J. Motheo, *Water. Res.* 41 (2007) 2969–2977.
- [42] D. Pavlov, *J. Electrochem. Soc.* 139 (1992) 3075–3080.
- [43] D. Pavlov, B. Monahov, *J. Electrochem. Soc.* 143 (1996) 3616–3629.
- [44] Y.Q. Cong, Z.C. Wu, *J. Phys. Chem. C* 111 (2007) 3442–3446.
- [45] N.D. Popović, J.A. Cox, D.C. Johnson, *J. Electroanal. Chem.* 455 (1998) 153–160.
- [46] P. Cañizares, F. Martínez, M. Díaz, J. García-Gómez, M.A. Rodrigo, *J. Electrochem. Soc.* 149 (2002) D118–D124.
- [47] N.D. Popović, D.C. Jonson, *Anal. Chem.* 70 (1998) 468–472.
- [48] M.E. Hyde, R.M.J. Jacobs, R.G. Compton, *J. Phys. Chem. B* 108 (2004) 6381–6390.
- [49] X.P. Zhu, S.Y. Shi, J.J. Wei, F.X. Lv, H.Z. Zhao, J.T. Kong, Q. He, J.R. Ni, *Environ. Sci. Technol.* 41 (2007) 6541–6546.
- [50] J.A. Dean, *Handbook of Organic Chemistry*, McGraw-Hill, New York, 1987.
- [51] M.B. Smith, J. March, *Advanced Organic Chemistry Reactions, Mechanisms, and Structure*, 5th ed., Wiley, New York, 2001.
- [52] J.G. Speight, *Lange's Chemistry Handbook Version 16th*, McGraw-Hill, New York, 2004.
- [53] A. Heintz, S. Kapteina, S.P. Verevkin, *J. Phys. Chem. A* 111 (2007) 6552–6562.
- [54] B. Sangchakr, T. Hisanaga, K. Tanaka, *J. Photochem. Photobiol. A: Chem.* 85 (1995) 187–190.
- [55] L. Oliviero, J. Barbier, D. Duprez, *Appl. Catal. B: Environ.* 40 (2003) 163–184.
- [56] P. Cañizares, C. Sáez, J. Lobato, M.A. Rodrigo, *Ind. Eng. Chem. Res.* 43 (2004) 1944–1951.
- [57] L.L. Houk, S.K. Johnson, J. Feng, R.S. Houk, D.C. Johnson, *J. Appl. Electrochem.* 28 (1998) 1167–1177.
- [58] X.Y. Li, Y.H. Cui, Y.J. Feng, Z.M. Xie, J.D. Gu, *Water. Res.* 39 (2005) 1972–1981.
- [59] D. Gandini, E. Mahe, P.A. Michaud, W. Haenni, A. Perret, Ch. Comninellis, *J. Appl. Electrochem.* 30 (2000) 1345–1350.
- [60] B. Nasr, G. Abdellatif, P. Cañizares, C. Sáez, M.A. Rodrigo, *Environ. Sci. Technol.* 39 (2005) 7234–7239.